Proc. Natl. Acad. Sci. USA
Vol. 90, pp. 5287–5291, June 1993
Biochemistry

Molecular and active-site structure of a *Bacillus* 1,3-1,4-β-glucanase

(hydrolase/inhibitor binding/protein conformation/x-ray crystallography/*in vitro* mutagenesis)

THOMAS KEITEL*, ORTWIN SIMON†‡, RAINER BORRISS†‡, AND UDO HEINEMANN*§

*Institut für Kristallographie, Freie Universität Berlin, Takustrasse 6, W-1000 Berlin 33, Federal Republic of Germany; †Institut für Genetik, Mikrobiologie und Biochemie, Humboldt-Universität Berlin, Warschauer Strasse 43-44, O-1017 Berlin, Federal Republic of Germany; and ‡Department of Physiology, Carlsberg Laboratory, Gamle Carlsberg Vej 10, DK-2500 Copenhagen Valby, Denmark

Communicated by Diter von Wettstein, December 24, 1992 (received for review November 23, 1992)

ABSTRACT **The three-dimensional structure of the hybrid *Bacillus* 1,3-1,4-β-glucanase (β-glucanase; 1,3-1,4-β-D-glucan 4-glucanohydrolase, lichenase, EC 3.2.1.73) designated H(A16-M) was determined by x-ray crystallography at a resolution of 2.0 Å and refined to an *R* value of 16.4% using stereochemical restraints. The protein molecule consists mainly of two seven-stranded antiparallel β-pleated sheets arranged atop each other to form a compact, sandwich-like structure. A channel crossing one side of the protein molecule accommodates an inhibitor, 3,4-epoxybutyl β-D-cellobioside, which binds covalently to the side chain of Glu-105, as seen in a crystal structure analysis at 2.8-Å resolution of the protein–inhibitor complex (*R* = 16.8%). That Glu-105 may be indispensible for enzyme catalysis by H(A16-M) is suggested by site-directed mutagenesis of this residue, which inevitably leads to an inactive enzyme.**

Since huge amounts of biomass are stored in the form of high molecular weight carbohydrates, polysaccharide depolymerizing enzymes are of considerable fundamental and biotechnological interest. An understanding of their function depends on the knowledge of the three-dimensional protein structures. Up until now, crystal structures of two cellulases (1, 2) and the solution structure of a cellulose-binding domain (3) have been reported. Several lysozymes (4–6) and α-amylases (7, 8) have also been structurally characterized. These different classes of enzymes show a wide variety of molecular architectures.

The 1,3-1,4-β-glucanases (1,3-1,4-β-D-glucan 4-glucanohydrolases, EC 3.2.1.73; also called lichenases and β-glucanases) represent a distinct family of glucanohydrolases in that they specifically cleave 1,4-β-D-glucosidic bonds in mixed-linked β-glucans that also contain 1,3-β-D-glucosidic linkages (9). Their natural substrates are β-glucans from grain endosperm cell walls or lichenan from the Islandic moss, *Cetraria islandica* (Fig. 1*A*). The β-glucanases secreted from different *Bacillus* strains share significant sequence homology (10–14) and also with the enzymes from *Clostridium thermocellum* and from *Fibrobacter succinogenes* (15, 16). They are distinct from the plant β-glucanases that are involved in the degradation of cell walls during the early stages of germination of cereal grains (17).

Covalently binding epoxyalkyl cellobiosides (Fig. 1*B*) have proven useful to study the active sites of glycoside hydrolases (18). The epoxide is the target of nucleophilic attack from catalytic residues, and the glucose moieties can be bound to subsites of the enzymes. For the *B. subtilis* β-glucanase, G4G-O-C_4 has been identified as the most effective covalently binding inhibitor (19).

Here we present the crystal structure analysis¶ of a hybrid 1,3-1,4-β-glucanase, H(A16-M), which contains amino acid residues 1–16 of the mature *Bacillus amyloliquefaciens* enzyme and residues 17–214 derived from the *Bacillus macerans* β-glucanase (20). Its complex with the covalently binding inhibitor G4G-O-C_4 serves to delineate the active-site region and to identify a catalytic amino acid residue of the H(A16-M) hybrid.

MATERIALS AND METHODS

Crystals of H(A16-M) were grown by a modification of the published procedure (21). The active protein (20) was dialyzed against 20 mM 2-(*N*-morpholino)ethanesulfonic acid (Mes) (pH 7.0)/2 mM EDTA. For crystallization, this solution was equilibrated against 12–16% (wt/vol) PEG 6000 by the hanging-drop vapor-diffusion method at room temperature. Crystals grown within 1 week belong to space group $P2_12_12_1$ with a = 70.22 Å, b = 72.56 Å, and c = 49.97 Å.

Addition of 2.5 mM calcium chloride to the mother liquor of these crystals leads to a change in cell parameters to a = 64.32 Å, b = 78.52 Å, and c = 39.30 Å without affecting either the space group or the diffraction quality. The calcium-form crystals were used for the collection of native and derivative diffraction data sets and for soaking with the inhibitor G4G-O-C_4 (Table 1). Soaking times were from 1 hr up to 4 days for heavy-atom derivatives and 4 days for the inhibitor.

Diffraction data sets were collected either on an Enraf Nonius CAD4 diffractometer equipped with an elongated counter arm or on a FAST television area detector system, both mounted on an FR 571 rotating anode generator producing CuK_α radiation. Isomorphous difference Patterson maps between the low-resolution native data set (Table 2) and derivative data sets U1 and Pt1 showed sharp Harker peaks. A U/Pt-cross derivative was used to establish the common origin of these derivatives, and difference Fourier syntheses served to locate the heavy-atom positions in other derivatives and to determine the handedness of the heavy-atom models.

The heavy-atom positions were refined by least squares analysis using only centric reflections. The electron density was improved by phase refinement, yielding a mean figure of merit of 80% and by subsequent solvent flattening (22) followed by phase combination. At this stage, the course of the polypeptide chain could be followed through an electron density map displayed on stacked minimaps, and most side chains could be identified.

A molecular model of H(A16-M), built with FRODO (23), was refined against 2.6-Å native diffraction data by using the slow-cooling simulated annealing procedure of the program

The publication costs of this article were defrayed in part by page charge payment. This article must therefore be hereby marked "*advertisement*" in accordance with 18 U.S.C. §1734 solely to indicate this fact.

Abbreviations: H(A16-M), hybrid 1,3-1,4-β-glucanase consisting of amino acids 1–16 of the *Bacillus amyloliquefaciens* enzyme and of amino acids 17–214 derived from the *Bacillus macerans* enzyme; G4G-O-C_4, (3,4)-epoxybutyl β-D-cellobioside.

§To whom reprint requests should be addressed.

¶The structure amplitudes and atomic coordinates of H(A16-M) and H(A16-M)·G4G-O-C_4 have been deposited in the Protein Data Bank, Chemistry Department, Brookhaven National Laboratory, Upton, NY 11973 (reference 1AYH, 1BYH). This information is available immediately.

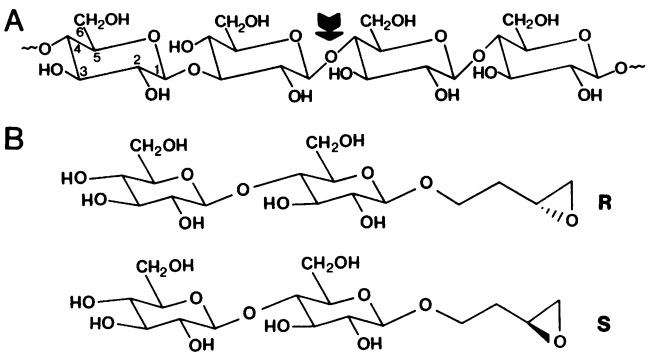

FIG. 1. (A) Portion of a β-glucan strand. The point of cleavage by β-glucanase at a 1,4-β-D-glucosidic bond is marked by an arrow. (B) Chemical structure of the covalently binding β-glucanase inhibitor 3,4-epoxybutyl β-D-cellobioside (G4G-O-C_4) in the 3R and 3S forms.

X-PLOR (24). The initial annealing temperature was set to 4000 K, and 120 refinement cycles were performed in six subsequent runs of X-PLOR. At the end of each run, model and experimental phases were combined with relative weights provided by the program SIGMAA (25). Then the improved map and the new coordinates were checked for correct fit and reasonable stereochemistry.

Finally, the resolution was extended to 2.0 Å and refinement was continued with PROFFT (26), converging with R = 16.4% after one calcium ion and 157 water molecules had been located from difference Fourier maps. The final protein model is well defined by electron density. Protein main-chain atoms have crystallographic B values between 2 and 34 $Å^2$ with a mean of 11.3 $Å^2$; the highest B values are observed in the side chains of Glu-1 and His-99, reaching a maximum of 54 $Å^2$ in the latter. All residues of H(A16-M) fall in the expected regions of the Ramachandran diagram except for Phe-10, Asn-125, Asp-161, and Asn-171, all of which adopt left-handed helix conformation.

Binding of the inhibitor G4G-O-C_4 to the H(A16-M) crystals left the unit cell parameters unchanged. A difference Fourier synthesis against the inhibitor diffraction data set with the refined phases of the free protein clearly showed the position and outline of G4G-O-C_4. Into this density a model of the inhibitor was built by using published coordinates (27). One run of simulated annealing starting from 2000 K and several subsequent cycles of conventional restrained least-squares refinement with X-PLOR yielded an R value of 16.8% against 8- to 2.8-Å resolution data after inclusion of the Ca^{2+} and 72 water molecules. For the atoms of the inhibitor, refinement with unit occupancies yielded B values comparable to those of the surrounding protein atoms.

Table 2. Refinement statistics for the H(A16-M) and H(A16-M)-G4G-O-C_4 crystal structures

	H(A16-M)	H(A16-M)-G4G-O-C_4
Resolution, Å	8–2.0	8–2.8
Crystals, no.	2	1
Reflections		
Measured, no.	27,023 (CAD4) 14,705 (FAST)	9,517 (FAST) —
Unique, no.	11,408	4,759
R_{merge}, %	5.7	3.2
Waters located, no.	157	72
R_{model}	16.4	16.8
rms Δ		
Bond distances, Å	0.017	0.018
Bond angle distances, Å	0.050	—
Bond angles, degree	—	3.56

$R_{model} = \Sigma_h|F_o - F_c|/\Sigma_h F_o$, the summation is over the h reflections used in refinement, and F_o and F_c are the observed and calculated structure amplitudes, respectively. rms Δ, root-mean-square deviation from ideal stereochemical parameters used in refinement. See the legend to Table 1. CAD4 and FAST refer to data-collection systems (see text).

Protein variants with substitutions in the positions corresponding to Glu-105 of mature H(A16-M) were generated by *in vitro* amplification of a 500-base-pair (bp) *Eco*RI–*Eco*RV DNA fragment of the *B. macerans* β-glucanase gene cloned into the pUC13 vector (28). The mutagenic oligonucleotide primer 951 contained equimolar amounts of all four nucleotides (N) in the position coding for the critical Glu-105 as well as the *Eco*RV recognition sequence (underlined) 5′ to the mixed base sequence: 5′ TTC GAT ATC TAT A/GNN ATC CCA TTG TGT 3′. The polymerase chain reaction (PCR) was performed with the direct sequencing primer 1224 (New England Biolabs), primer 951, and plasmid pUC13-M (29) as template. The amplified DNA fragment was cut with *Eco*RI and *Eco*RV and used to substitute the corresponding wild-type sequence in pUC13-M. Mutated plasmids were transformed into *Escherichia coli* DH5α cells and sequenced (30). Expression of β-glucanase activity was tested on lichenan agar plates (29).

The inhibitor used in this study, G4G-O-C_4, was synthesized by published procedures (19) as a mixture of the 3R and 3S stereoisomers.

RESULTS AND DISCUSSION

Tertiary Structure. The hybrid β-glucanase H(A16-M) folds into one compact globular domain consisting almost

Table 1. X-ray diffraction data used for structure analysis of H(A16-M)

		Derivative					
	Native	U1	Pt1	U/Pt	U2	Pt2	Hg
Resolution, Å	2.6	3.0	2.8	2.8	2.6	2.8	3.0
Reflections							
Measured, no.	14,705	11,435	11,195	9,517	13,713	12,872	14,096
Unique, no.	8984	7517	7702	6997	9538	9763	9948
R_{merge}, %	3.7	4.5	2.7	3.8	3.4	3.6	3.8
f.i.d., %	—	19.6	24.4	15.2	29.0	20.4	23.8
Sites, no.	—	1	2	1 U/2 Pt	2	3	3
$\langle f_h/\varepsilon \rangle$	—	3.33	1.46	1.82	2.71	2.11	1.35
R_{Cullis}, %	—	51	70	67	50	62	71

Derivatives: U1, $UO_2(NO_3)_2$ (soaked at pH 7.0); Pt1, K_2PtCl_4 (pH 7.0); U/Pt, $UO_2(NO_3)_2/K_2PtCl_4$ (pH 7.0); U2, $UO_2(NO_3)_2$ (pH 8.5); Pt2, K_2PtCl_4 (pH 8.5); Hg, $Hg(OAc)_2$ (pH 7.0). $R_{merge} = \Sigma_{h,i}|\langle I_h \rangle - I_{h,i}|/\Sigma_{h,i} I_{h,i}$, the sum over i measurements of intensities $I_{h,i}$ in h independent reflections. The resolution limit used for phasing was determined by isomorphism and was usually lower than that to which data were collected; f.i.d. = $\Sigma_h|F_p - F_{ph}|/\Sigma_h F_p$, fractional isomorphous difference between structure amplitudes F_p of the native protein crystal and F_{ph} of the heavy atom derivative; f_h, heavy-atom structure factor; ε, isomorphous lack-of-closure error; $R_{Cullis} = \Sigma_h||F_{ph} \pm F_p| - |f_{h(calc)}||/\Sigma_h|F_{ph} - F_p|$.

exclusively of β-pleated sheet and surface loops (Fig. 2). The molecule has a slightly elongated shape with a prominent cleft crossing one side. This cleft originates from the twist and bending of two β-sheets arranged atop each other in a sandwich-like manner and from loop regions including one complete α-helical turn and a segment of three consecutive residues in α-helical conformation. The interior of the protein between the β-sheets is packed with hydrophobic residues. The molecular architecture of H(A16-M) bears no similarity with the known structures of cellulases, lysozymes, or amylases (1–8). However, the plant lectins show the same "jelly-roll" β-barrel topology in their subunits (33).

In H(A16-M), the polypeptide chain is folded into two strictly antiparallel, seven-stranded β-sheets with the usual left-handed twist. The chain crosses several times between the sheets. Both sheets are curved to give rise to a convex and

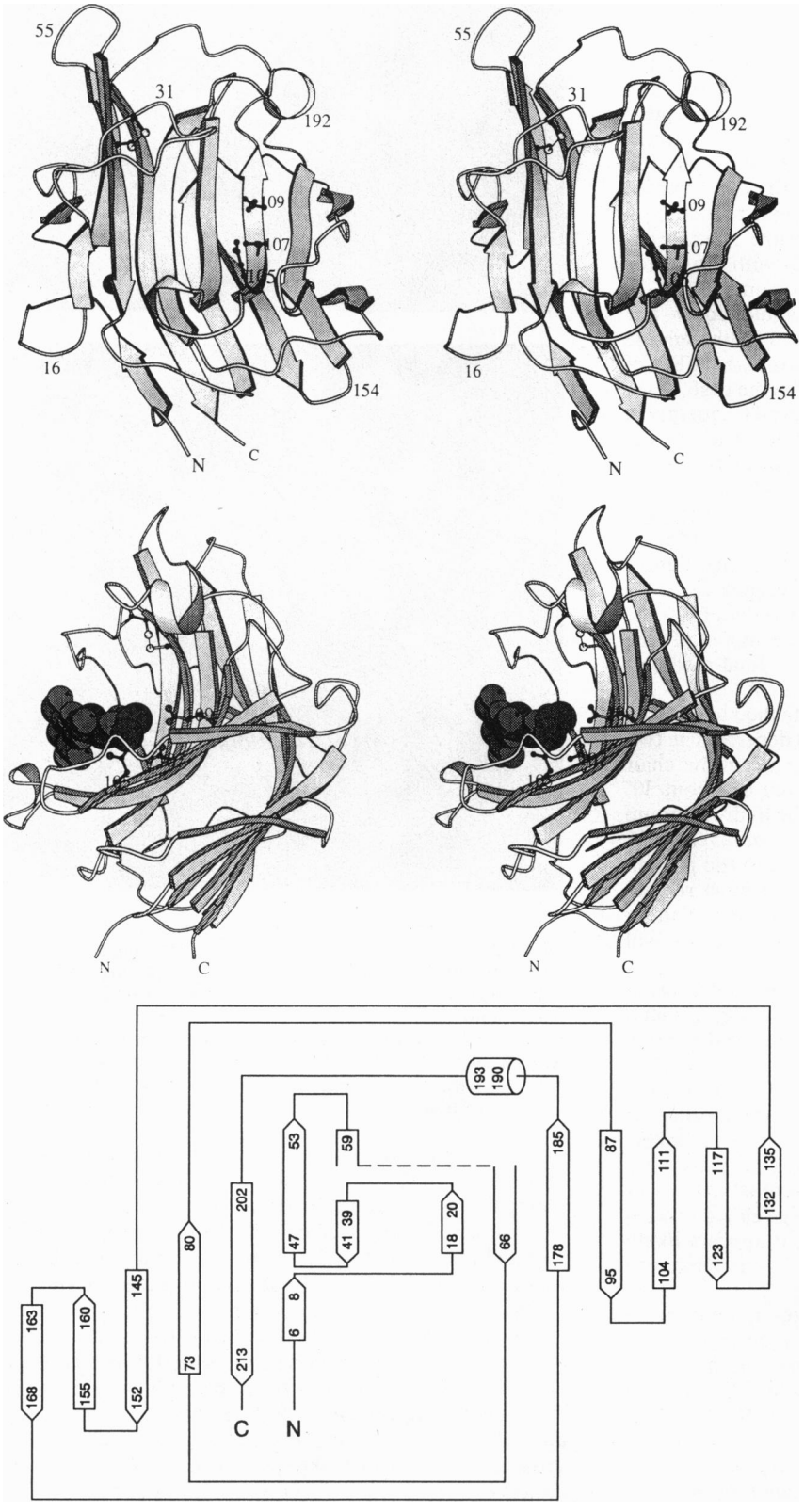

FIG. 2. (*Top*) Stereo drawings of the molecular structure of H(A16-M) oriented approximately perpendicular to the β-sheet sandwich. The course of the polypeptide chain is indicated by a smooth line, arrows mark β-strands, and a piece of wound ribbon represents the short α-helical segment. The single disulfide bond and the side chains of Glu-105, Asp-107, and Glu-109 in the active site are explicitly included. The calcium ion (dark sphere) is partly hidden beneath the second strand from the left in the top β-sheet. Drawn with MOLSCRIPT (31). (*Middle*) Binding of G4G-O-C_4 to the active site of H(A16-M). (*Bottom*) Sketch of the H(A16-M) secondary structure as analyzed with the program DSSP (32). Arrows and a cylinder mark β-strands and the α-helix, respectively. The bottom β-sheet is on the left side, and the top sheet is shown at the right.

a concave side of the molecule. Substrates bind to the cleft on the concave side, whereas a calcium ion is bound with nearly perfect octahedral geometry on the convex face of the protein, coordinating to the backbone carbonyl oxygen atoms of Pro-9, Gly-45, and Asp-207, a carboxylate oxygen of Asp-207, and two water molecules. Amino and carboxyl termini are linked to adjacent strands in the convex β-sheet and are very close in space. The single disulfide bond attaches the extended loop region around Cys-32 to Cys-61 in the convex β-sheet.

Active-Site Structure. The cleft on the concave side of the H(A16-M) molecule is ideally suited for the binding of oligosaccharide substrates. It is lined with mainly aromatic amino acid side chains on one wall and with acidic residues on the other. Especially conspicuous is the polypeptide stretch between Trp-103 and Glu-109 from which the tryptophan and three acidic side chains point towards the left (Fig. 3 *Upper*). Asp-104, Ile-106, and Ile-108 are oriented away from the active-site cleft, the latter two partaking in hydrophobic interactions in the protein interior. The carboxylate of Glu-105 forms two hydrogen bonds with the indole nitrogen of Trp-103 (2.8 Å) and a side-chain oxygen of Asp-107 (2.5 Å). The latter hydrogen bond would require one of the two acidic side chains to be protonated. Although the pH value of crystallization, 7.0, is far from the pK_a of carboxylates in aqueous solution, this may be the case, since carboxyl–carboxylate interactions are observed frequently in protein crystal structures (34)—for example, in the active site of cellobiohydrolase II (2). The observed hydrogen-bonding interactions could help to position the Glu-105 carboxylate group and to optimize its acidity for a function in catalysis.

Inhibitor Binding. The inhibitor G4G-O-C_4 was diffused into crystals of H(A16-M) by addition to their mother liquor. Fig. 3 *Lower* shows the unbiased initial difference electron-density map, obtained by using the diffraction data from the inhibitor-soaked crystal and phases from the model of free H(A16-M). Superimposed on this map is the final model of the bound G4G-O-C_4 after structure refinement.

The inhibitor appears to be covalently attached to the side chain of Glu-105 as indicated by contiguous density. The two glucose molecules of the cellobiose moiety are in the chair conformation, their best planes being twisted by about 30° with respect to each other. The position of the hydroxy group of the β-hydroxy ester presumably formed is not revealed by electron density. Since G4G-O-C_4 was added to the protein as a mixture of the *R* and *S* stereoisomers, it must remain unclear at present whether the enzyme binds one of these preferentially, as expected (18), and which isomer this will be.

The conformation of H(A16-M) and the geometry of its active site remain nearly unchanged upon binding of G4G-O-C_4 (see Fig. 2). The cellobioside unit is bound to the active site by hydrogen bonds between its hydroxyl groups and the side chains of amino acids Glu-63, His-99, Tyr-24, and Asn-26. The latter residue is especially important, since its amide group contacts both glucose moieties. The butyl linker, spanning the presumed catalytic site, makes no close contacts to active-site atoms of H(A16-M). There is no contact between the bound G4G-O-C_4 and symmetry-related protein molecules in the crystal lattice. Therefore, it appears likely that the inhibitor binding seen in the crystal is very similar to that taking place in solution.

Amino Acid Substitutions in Glu-105. Site-directed mutagenesis by PCR yielded mutants of the *B. macerans* β-glucanase with the following amino acid substitutions in the position corresponding to H(A16-M) Glu-105: Glu-105 → Asp, Glu-105 → Asn, Glu-105 → Ala, Glu-105 → Leu, Glu-105 → Pro, Glu-105 → Arg, Glu-105 → His, Glu-105 → Cys, Glu-105 → Ser, and Glu-105 → Tyr (28). All enzyme variants were without detectable β-glucanase activity as judged by lichenan agar plates and by the quantitative enzyme assay (29). Polypeptides with the expected relative molecular weight could be detected by SDS/PAGE of periplasmic cell fractions of *E. coli* cells transformed with the mutated plasmids. This is taken as evidence that the substitutions in position 105 did not abolish protein synthesis.

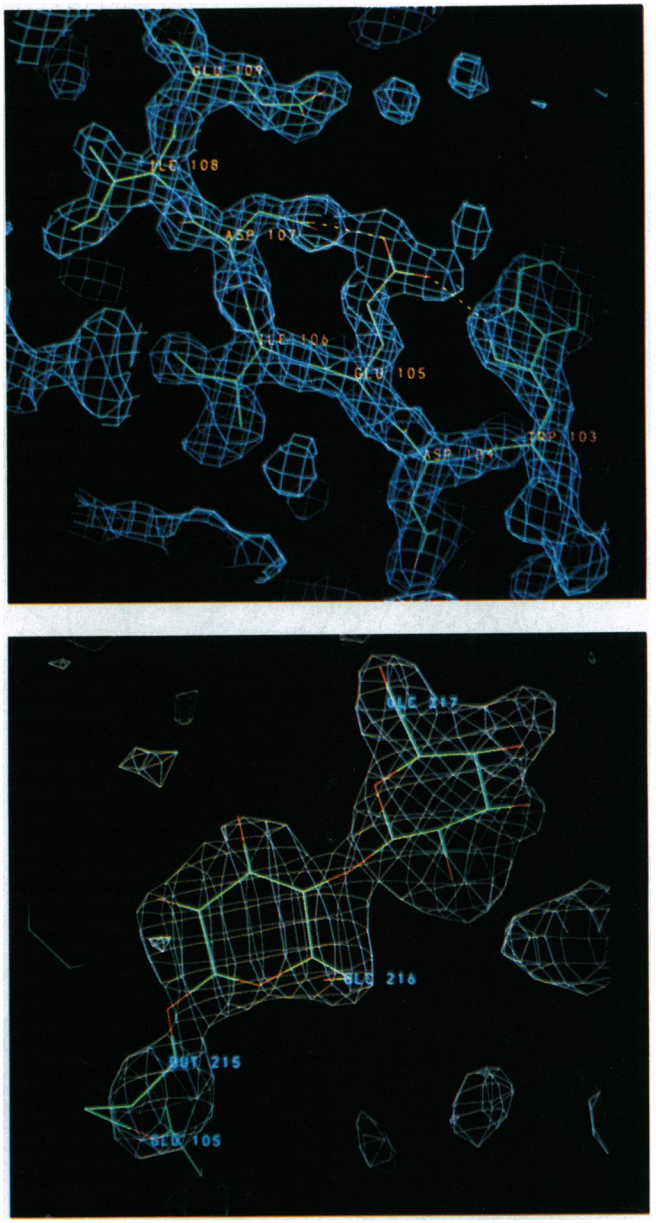

FIG. 3. (*Upper*) Polypeptide segment Trp-103 to Glu-109 of H(A16-M) superimposed onto a 2.0-Å resolution electron density map computed with coefficients $(2F_o - F_c)\exp(-i\alpha_c)$ and contoured at 0.65 electron per Å^3. (*Lower*) Final model of G4G-O-C_4 superimposed onto difference electron density computed with the 2.8-Å resolution structure amplitudes from the inhibitor-soaked crystal and with phases from the free H(A16-M) model. The density is contoured at 0.18 electron per Å^3. But, butyl linker; Glc, glucose residues (the inhibitor residue starts at 215).

On the contrary, protein variants with substitutions of the adjacent residue Asp-104 were found to have considerable residual activity (28). This is in line with the crystal structure, since Asp-104 points away from the active-site channel.

Functional Implications. The crystal structures of H(A16-M) and H(A16-M)·G4G-O-C_4 strongly suggest that β-glucan hydrolysis by the enzyme takes place in the channel spanning the concave side of the protein molecule and that Glu-105, to

which the inhibitor is covalently bound, is a catalytic residue. The assignment of an important role in catalysis to Glu-105 is supported by results from the site-directed mutagenesis of the residues Asp-104 and Glu-105 in the *B. macerans* β-glucanase, which is identical to H(A16-M) except for 10 sequence positions near the amino terminus (20). In this enzyme, Glu-105 is indispensible for catalysis, whereas Asp-104 is not. Asp-104 points away from the catalytic site in H(A16-M) and may thus be substituted by different residues.

The same type of experiment has been reported for the β-glucanase from *Bacillus licheniformis* (35). Here again, site-directed mutagenesis of the glutamic acid residue corresponding to Glu-105 of H(A16-M) abolishes enzyme activity. In addition, peptide analysis has shown the equivalent glutamic acid of the *B. subtilis* β-glucanase to covalently bind G4G-O-C_4 (36). This combined evidence suggests that (*i*) the inhibitor binding observed in the crystal structure of H(A16-M)·G4G-O-C_4 is not a crystal artefact, (*ii*) Glu-105 is a catalytic residue that might be responsible for nucleophilic attack on the substrate, and (*iii*) the mode of protein–substrate interaction deduced for H(A16-M) is likely to be generally valid for *Bacillus* β-glucanases and possibly also for other homologous bacterial enzymes. Grain β-glucanases are unrelated by sequence and are known to interact differently with substrate polysaccharide strands (18).

At the resolution of 2.8 Å at which the protein–inhibitor complex is known at present, fine details of substrate recognition and enzyme catalysis must remain obscure. This especially concerns the stereochemical course of the reaction, which will become clearer when the missing hydroxyl group from the β-hydroxy ester at Glu-105 can be located. We have recently collected x-ray data from a H(A16-M)·G4G-O-C_4 crystal diffracting well beyond 2-Å resolution that may resolve this ambiguity.

We are indebted to Drs. O. Olsen and K. K. Thomsen (Carlsberg Laboratory) for their generous support and especially for the sequencing of all mutants obtained so far. O. Politz and S. Strigel (Humboldt University, Berlin) are thanked for the preliminary biochemical characterization of mutant β-glucanases and for technical support in the purification of hybrid enzymes. We are grateful to D. Donner for synthesis of the inhibitor and to Prof. W. Saenger for advice and the use of equipment. This work was supported by the Deutsche Forschungsgemeinschaft through Grants He 1318/9-1 and Bo1113/1-1, by the Fonds der Chemischen Industrie, and by the Danish Programme for Food Technology, Project 6028.

1. Juy, M., Amit, A. G., Alzari, P. M., Poljak, R. J., Claeyssens, M., Beguin, P. & Aubert, J.-P. (1992) *Nature (London)* **357**, 89–91.
2. Rouvinen, J., Bergfors, T., Teeri, T., Knowles, J. K. C. & Jones, T. A. (1990) *Science* **249**, 380–386.
3. Kraulis, P. J., Clore, G. M., Nilges, M., Jones, T. A., Pettersson, G., Knowles, J. & Gronenborn, A. (1989) *Biochemistry* **28**, 7241–7257.
4. Phillips, D. C. (1967) *Proc. Natl. Acad. Sci. USA* **57**, 484–495.
5. Artymiuk, P. J. & Blake, C. C. F. (1981) *J. Mol. Biol.* **152**, 737–762.
6. Anderson, W. F., Grütter, M., Remington, S. J., Weaver, L. H. & Matthews, B. W. (1981) *J. Mol. Biol.* **147**, 523–543.
7. Matsuura, Y., Kusunoki, M., Harada, W. & Kakudo, M. (1984) *J. Biochem. (Tokyo)* **95**, 697–702.
8. Buisson, G., Duée, E., Haser, R. & Payan, F. (1987) *EMBO J.* **6**, 3909–3916.
9. Anderson, M. A. & Stone, B. A. (1975) *FEBS Lett.* **52**, 202–207.
10. Murphy, N., McConnell, D. J. & Cantwell, B. A. (1984) *Nucleic Acids Res.* **12**, 5355–5367.
11. Hofemeister, J., Kurtz, A., Borriss, R. & Knowles, J. (1986) *Gene* **49**, 177–187.
12. Borriss, R., Buettner, K. & Maentsaelae, P. (1990) *Mol. Gen. Genet.* **222**, 278–283.
13. Lloberas, J., Perez-Pons, J. A. & Querol, E. (1991) *Eur. J. Biochem.* **197**, 337–343.
14. Gosalbes, M. J., Perez-Gonzalez, J. A., Gonzalez, R. & Navarro, A. (1991) *J. Bacteriol.* **173**, 7705–7710.
15. Schimming, S., Schwarz, W. & Staudenbauer, W. L. (1992) *Eur. J. Biochem.* **204**, 13–19.
16. Teather, R. M. & Erfle, J. D. (1990) *J. Bacteriol.* **172**, 3837–3841.
17. Fincher, G. B., Lock, P. A., Morgan, M. M., Lingelbach, K., Wettenhall, R. E. H., Mercer, J. F. B., Brandt, A. & Thomsen, K. K. (1986) *Proc. Natl. Acad. Sci. USA* **83**, 2081–2085.
18. Høj, P. B., Rodriguez, E. B., Iser, J. R., Stick, R. V. & Stone, B. A. (1991) *J. Biol. Chem.* **266**, 11628–11631.
19. Høj, P. B., Rodriguez, E. B., Stick, R. V. & Stone, B. A. (1989) *J. Biol. Chem.* **264**, 4938–4947.
20. Olsen, O., Borriss, R., Simon, O. & Thomsen, K. K. (1991) *Mol. Gen. Genet.* **225**, 177–185.
21. Keitel, T., Granzin, J., Simon, O., Borriss, R., Thomsen, K. K., Wessner, H., Höhne, W. & Heinemann, U. (1991) *J. Mol. Biol.* **218**, 703–704.
22. Wang, B. C. (1985) *Methods Enzymol.* **115**, 90–112.
23. Jones, T. A. (1978) *J. Appl. Crystallogr.* **11**, 268–272.
24. Brünger, A. T., Kuriyan, J. & Karplus, M. (1987) *Science* **235**, 458–460.
25. Read, R. J. (1986) *Acta Crystallogr.* **A42**, 140–149.
26. Hendrickson, W. A. (1985) *Methods Enzymol.* **115**, 252–270.
27. Moncrief, J. W. & Sims, S. P. (1969) *J. Chem. Soc. D*, 915–916.
28. Olsen, O. (1990) Ph.D. thesis (Aarhus Univ., Aarhus, Denmark).
29. Borriss, R., Olsen, O., Thomsen, K. K. & von Wettstein, D. (1989) *Carlsberg Res. Commun.* **54**, 41–54.
30. Zhang, H., Scholl, R., Browse, J. & Somerville, C. (1988) *Nucleic Acids Res.* **16**, 1220.
31. Kraulis, J. P. (1991) *J. Appl. Crystallogr.* **24**, 946–950.
32. Kabsch, W. & Sander, C. (1983) *Biopolymers* **22**, 2577–2637.
33. Einspahr, H., Parks, E. H., Suguna, K., Subramanian, E. & Suddath, F. L. (1986) *J. Biol. Chem.* **261**, 16518–16527.
34. Sawyer, L. & James, M. N. G. (1982) *Nature (London)* **295**, 79–80.
35. Planas, A., Juncosa, M., Lloberas, J. & Querol, E. (1992) *FEBS Lett.* **308**, 141–145.
36. Høj, P. B., Condron, R., Traeger, J. C., McCauliffe, J. C. & Stone, B. A. (1992) *J. Biol. Chem.* **267**, 25059–25066.